LA-UR--93-223

DE93 007377

TITLE: **TRACER EXPERIMENT RESULTS DURING THE LONG-TERM FLOW TEST OF THE FENTON HILL RESERVOIR**

AUTHOR(S): **NELSON E. V. RODRIGUES**
BRUCE A. ROBINSON
DALE COUNCE

SUBMITTED TO: **EIGHTEENTH ANNUAL WORKSHOP GEOTHERMAL RESERVOIR ENGINEERING STANFORD UNIVERSITY**

DISCLAIMER

MASTER

Los Alamos Los Alamos National Laboratory
Los Alamos, New Mexico 87545

Tracer Experiment Results During the Long-Term Flow Test of the Fenton Hill Reservoir

Nelson E. V. Rodrigues
CSM Associates
Rosemanowes, Penryn, Cornwall
TR10 9DU, U. K.

Bruce A. Robinson, and Dale A. Counce
Los Alamos National Laboratory
Earth and Environmental Sciences Division
Los Alamos, New Mexico, 87545

Abstract

Three chemical tracer experiments and one extended injection of fluid low in concentration of dissolved species have been carried out during the Long Term Flow Test (LTFT) of the Fenton Hill Hot Dry Rock (HDR) reservoir. The tracer tests results illustrate the dynamic nature of the flow system, with more fluid traveling through longer residence time paths as heat is extracted. The total fracture volumes calculated from these tests allow us to determine the fate of unrecovered injection fluid, examine the pressure-dependence of fracture volume, and, through a comparison to the hydraulic performance, postulate a model for the nature of the pressure drops through the system. The Fresh Water Flush (FWF) test showed that while no dissolved specie behavior is truly conservative (no sources or sinks), several breakthrough curves are well explained with a pore fluid displacement model. Other dissolved components are clearly influenced by dissolution or precipitation reactions. Finally, the transient response of the chemistry during the FWF to an increase in production well pressure showed that some fractures connected to the production well preferentially open when pressure is raised.

Introduction

The HDR concept has been under investigation at Los Alamos since the early 1970's at the Fenton Hill site. The site is located on the west flank of the Valles Caldera in the Jemez Mountains of northern New Mexico. On April 10, 1992 a Long Term Flow Test (LTFT) was initiated with the objective of demonstrating that heat can be extracted from the reservoir for a sustained period of time without produced fluid temperature decline. The operational goal was to maintain continuous circulation for a period of one to two years. However, technical problems occurred which necessitated a shut down at the beginning of August to replace the high pressure injection pumps. Injection resumed on August 14, and production resumed on the 19th, though at somewhat lower flow rates than during the period April 10 - July 30.

During this phase of the LTFT, three tracer tests have been performed using p-toluenesulphonic acid (p-TSA) and sodium fluorescein. The fluorescein apparently underwent some thermal degradation in the reservoir. The results discussed here are only for p-TSA tracer tests as these were inert or conservative tracer tests. A summary of test dates and tracer injection masses is provided in Table 1.

TABLE 1. Summary of p-TSA tracer tests.

test	date	mass of tracer injected
first	May 18, 1992	162.1 g
second	July 7, 1992	181.1 g
third	Sept 1, 1992	181.1g

Tracer tests in HDR systems are invariably pulse inputs of a large mass of tracer over a short period of time. However, a step input of a tracer can be simulated in a Fresh Water Flush (FWF) test, in which the following steps are carried out: 1) the system is circulated in closed-loop until quasi-equilibrium is reached with respect to dissolved species in the produced water, 2) circulation is suddenly changed to open-loop with the injection of "fresh water" from a source of fluid low in concentration of dissolved species; and 3) the concentration versus time of dissolved species is measured in the produced fluid. Then, the outlet concentration since the beginning of open-loop circulation can be interpreted as a step tracer test. If a dissolved specie is not produced or consumed by any source or sink mechanism, then its behavior can be predicted from the tracer response curve. Any deviations from this predicted behavior is then evidence of a source or sink within the reservoir.

During the long term circulation test at Fenton Hill one FWF test was conducted essentially simultaneously with the p-TSA tracer test of September 1. The test lasted about 160 hours, during which time fresh water from a domestic water well was injected while the produced fluid was vented temporarily to a storage pond. The present study summarizes the tracer tests and this FWF test, comparing the two to draw inferences about the nature of flow and the source of dissolved species in the circulating fluid.

Analysis of tracer data

The following analyses of the tracer data are presented below:

- calculation of the external and internal residence time distributions ($f(t)$ and $\chi(t)$ respectively, e.g Robinson and Tester, 1986);
- analysis of reservoir conditions during the three tests to infer possible changes in reservoir flow patterns throughout this period;
- comparison of the variation of the integral mean volume with the "water loss"; and

- under the assumption of a simplified geometry, analysis of the variation in volume and area of reservoir with time.

Figure 1 shows the experimentally determined tracer breakthrough curves for the three tracer tests. To interpret these results quantitatively, we define the following functions. First, f(t)dt is the fraction of particles in the exit stream with residence time between t and t+dt, and is given by $f(t) = qC(t)/m_p$, where q is the mass flow rate of fluid and m_p is the mass of tracer injected. Then, $\chi(t)dt$ is the fraction of particles *inside the system* that will eventually have a residence time between t and t+dt, and is equal to $tf(t)/\tau$, where τ is the mean residence time, computed from a first-moment integration of f(t).

When we plot the cumulative distributions of these two functions (F(t) is the cumulative distribution for f(t) and X(t), also known as the internal residence time distribution (RTD), is the cumulative distribution of $\chi(t)$) against one another, we obtain a quantitative picture of the nature of the flow paths within the reservoir. Figure 2 is such a plot for the three tracer tests. Plotting the data in this way shows, for example, that in the first two tracer tests, the 50% of the injected fluid that is traveling fastest sweeps through only 12% of the internal fluid volume of the reservoir (obtained from the point on the curve at 0.5, 0.12). Thus, although there is a tendency for fluid to short circuit directly between the wells, a significant percentage of the fluid sweeps through a very large volume.

Note also that the total fluid volume (computed as the mean residence time times volumetric flow rate) increased during operation at constant flow conditions between the first and second tests (Table 2). There is a shift to longer residence times, with fluid possibly circulating through a greater number of flow paths. The alternative model is that the increased fluid flow volume is simply due to some additional dilation of existing flow paths, without accessing additional rock. It is impossible to distinguish between the models, although we note that curves for the first two tracer tests in Figure 2 are almost identical despite the shift to longer residence times and larger fluid volumes. This might suggest that the existing flow paths are more dilated with no change in the flow distribution through the rock mass.

The third test was conducted at lower flow rates and pressures, and the resulting total fracture volume was considerably lower. Furthermore, Figure 2 indicates that any given fraction of the injected fluid travels through a greater fraction of the total volume in the third test than in the previous two tests. One explanation is that at lower pressures, some joints that previously conducted fluid no longer are open enough to do so. Thus the joints that continue to transmit fluid have smaller volume, and fluid does not percolate as readily through the long-residence-time, tortuous flow paths. Greater rock volumes are almost certainly accessed at the higher pressure conditions.

Another issue that has interested HDR researchers for many years is the fate of the injected fluid that is not recovered at the production well. These tracer results show that during steady flow operation between the first and second tests, the volume of "active flow paths" (those that transmit fluid between the wells) increased by 520 m^3, compared to a total fluid consumption of 3400 m^3 during the same period. Thus, during this test about 16% of the "water loss" actually resulted in increased volume of active flow paths, with the remaining fluid probably diffusing into rock between the fractures or at the boundary of the fractured reservoir.

FIGURE 1. Normalized tracer breakthrough curves for the p-TSA experiments.

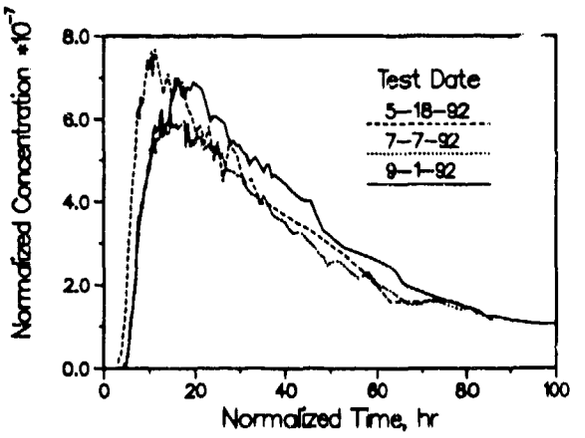

TABLE 2. Integral Mean Volume Variation

Test	Integral Mean Volume	Variation in volume
First	2246 m^3	
Second	2766 m^3	+520 m^3
Third	2044 m^3	-722 m^3

FIGURE 2. Internal volume fraction versus fluid flow fraction for the three tracer tests.

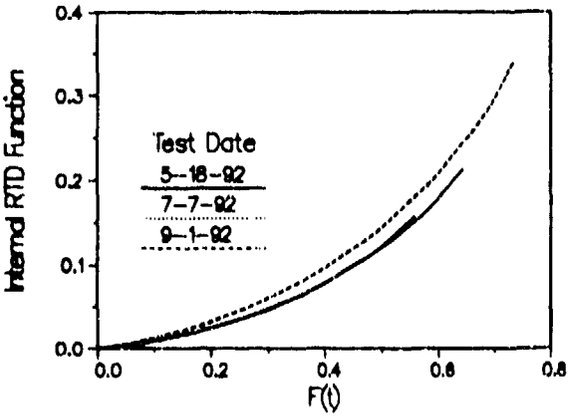

Inferences about the nature of flow and pressure drop through the reservoir can be made by estimating joint apertures, using both pressure drop and tracer information. Information needed for the pressure drop computation and the

corresponding assumptions used for the calculation are: 1) flow velocity based on the known distance between the wells and a measured transit time based on the first arrival of the tracer; 2) mean joint spacing of 20 m based on the heat transfer study of Robinson and Kruger (1992); 3) rock volume dimensions of 150 x 80 x 240 m cut by a three-dimensional array of evenly spaced fractures; and 4) tracer-determined total fracture volume of 2246 m^3 (first tracer test). The resulting apertures obtained are summarized in Table 3 below.

TABLE 3. Estimates of joint apertures.

aperture (m)	reference
$2.1*10^{-4}$	cubic law aperture (Snow, 1969)
$3.0*10^{-5}$	friction law aperture (Abelin et al., 1987)
$2.0*10^{-5}$	radial flow (Witherspoon et al., 1980)
$5.2*10^{-3}$	storage aperture

The first three aperture values are so-called hydraulic apertures, based only on the pressure drop across the reservoir and assumed fracture and flow parameters without consideration of the tracer-determined fracture volume. Contrast these values with the storage aperture, the value obtained using the total fracture volume and the assumed fracture geometry. The actual storage volume in the joints is much larger than would be suggested based on the pressure drop through the reservoir. Even assuming a larger reservoir and closer fracture spacing, the large discrepancy remains. This result is very typical of flow through fracture rock, and is thought to be due to the fact that the hydraulic aperture is dominated by flow constrictions (small apertures) that the fluid is forced to traverse. By contrast, the storage aperture is a straight average of all apertures encountered by flowing fluid. Conceptually, the hydraulic system in the reservoir is one of large pressure drops through some crucial fractures or portions of fractures of small aperture, with fluid experiencing almost no pressure drop through the large aperture fractures that contribute most to the fluid storage volume.

Fresh Water Flush (FWF) Test

Since the concentration of almost all dissolved species is lower in the fresh water than in the circulating fluid during a FWF experiment, the results are analyzed as a *negative step tracer test*, and the washout function, W(t), can be directly calculated from the following expression:

$$W(t) = \frac{C(t) - C_i}{C_o - C_i} \qquad (1)$$

where C(t) is the outlet concentration at time t, C_i is the concentration of the injected fluid, and C_o is initial produced fluid concentration at the beginning of the FWF.

Analysis of a FWF test must account for the following possibilities, each of which could result in a concentration time response that differs from that of a conservative tracer:

- a constant source of the specie in the form of indigenous pore fluid of high concentration that is swept into the produced fluid as new flow paths are accessed;
- production or consumption of the specie via rock-water interactions in the reservoir. Some possible processes are dissolution of minerals, ion exchange, or interaction with pore fluid. In each case the results can be analyzed assuming a source or sink of the specie;
- reversible adsorption of the specie onto the rock surface. Here the specie is delayed compared to one that does not undergo sorption.

Since it will be shown that many species appear to have a source in the reservoir, we develop a method for interpreting the data in the presence of a source. Assuming a constant source of solute, the dimensionless concentration may be obtained from a revised form of Eqn. (1):

$$\bar{C} = \frac{(C'(t) - C_i)}{(C'_o - C_i)} \qquad (2)$$

where $C'(t) = C(t) + C_s$, $C'_o = C_o + C_s$, and C_s is the source concentration.

Using these equations, the source concentration can be calculated as follows:

$$C_s = \frac{(C'(t) - C_i - W(t) \times (C_o - C_i))}{1 - W(t)} \qquad (3)$$

This value is actually a weighted source concentration, equal to the actual concentration of the added fluid (assumed to be pore fluid in this discussion) times the ratio of the pore fluid flow rate to the total flow rate. If the source of solute is indeed from pore fluid, then a mass balance yields:

$$q \times C'(t) = q_o \times C(t) + q_p \times C_p \qquad (4)$$

$$q \times C'_o = q_o \times C_o + q_p \times C_p \qquad (5)$$

where q_p is the mass flow rate of pore fluid, C_p is the concentration of the pore fluid, and $q = q_o + q_p$. Calculating the value of q_p and using Eqn. (2), the following relation is obtained:

$$q_p = C_i \times \frac{q}{(\bar{C}_p - C_i)} \qquad (6)$$

During the FWF test, chemical analyses were made of the following dissolved species: Al, As, B, Br, Ca, Cl, F, Fe, HCO_3, Li, Mg, Na, NO_3, PO_4, Si, SO_4, Sr, and Total Dissolved Solids (TDS).

To analyze the test, the washout function W(t) for the p-TSA tracer test was first derived from an integration of the p-TSA tracer response curve. Then, the washout response of each specie was computed using Eqn. (1), with C_i obtained from a chemical analysis of the injected fresh water and C_o determined from an average of all concentrations measured during the 15 hours before breakthrough of the fresh water (values for C_o are listed in Table 4). The comparison of the tracer-determined washout function with the dissolved species B, Br, Cl, K, Li, Na, SO_4, Sr and TDS are presented in Figures 3 to 5 and discussed below.

A truly conservative species would have a concentration-time response coincident with W(t) determined from a tracer experiment. As shown in the figures, none of the species analyzed behaved as a truly conservative tracer. In many cases, the deviation of the dimensionless concentration curves from the tracer-determined W(t) curve can be explained assuming a constant source of the specie. Using the mathematical development outlined above, the source concentration C_s for B, Br, Cl, Li, Na, K, SO_4, Sr have been calculated: the results are given in Table 5.

TABLE 4. Initial Concentrations C_o at the start of the FWF (ppm)

B	Br	Cl	K	Li	Na
46.7	6.7	1371	106	17.4	1107
SO4	**Sr**	**T.D.S.**			
398	0.91	3947			

FIGURE 3. Dimensionless concentrations of B, Br, and Cl during the FWF

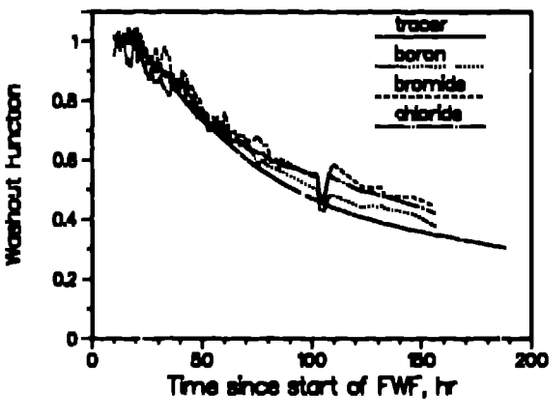

FIGURE 4. Dimensionless concentrations of K, Li, and Na during the FWF

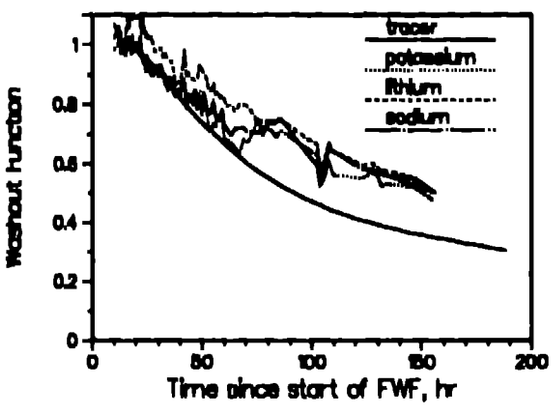

FIGURE 5. Dimensionless concentrations of SO_4, Sr, and TDS during the FWF.

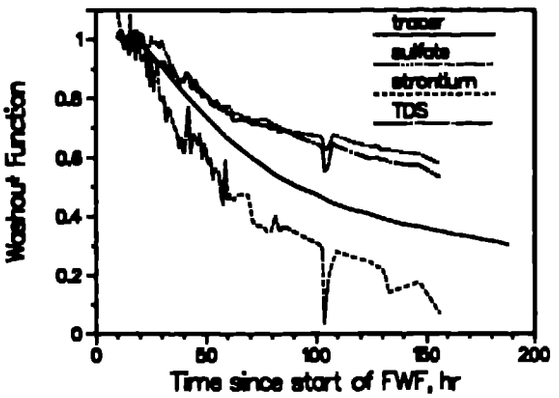

FIGURE 6. Fluoride ion behavior during the FWF.

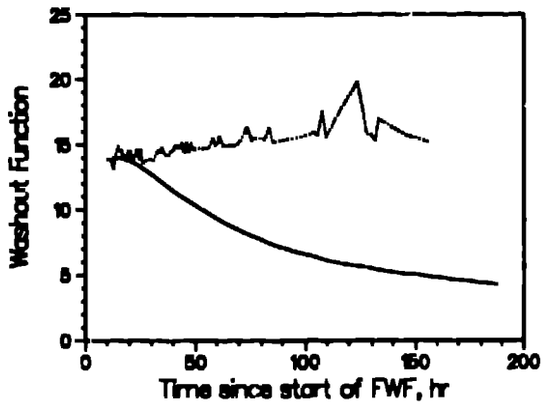

TABLE 5. Calculated average source concentrations (ppm)

B	Br	Cl	Li	Na	K
11.7	1.5	273.7	6.0	423.4	35.6
SO_4	**Sr**	**TDS**			
164.5	-0.18	1310			

Of the species listed in the table, the origin of boron and chlorine is almost certainly pore fluid, because there are no minerals in the host rock that can be a source for these elements (e. g. Laney et al, 1981). Using as the composition of the pore fluid the composition of downhole samples developed during the development of EE-2 (Table 6, from Grigsby et al, 1989), the approximate contribution of pore fluid to the produced flow can be calculated. The results for several of the species, in the form of percent of the outlet flow that was derived from pore fluid, is given in Table 7.

TABLE 6. Approximate Pore Fluid Composition in ppm (Grigsby et al, 1989)

pH	Conductivity(uS)	SiO_2	Na	K	Li	Ca
6.46	18000	435	3310	401	76.1	94.0
Mg	**B**	**SO_4**	**Cl**	**HCO_3**	**F**	**Br**
3.0	178.0	64	5870	692	6.1	42.3

TABLE 7. Percent pore fluid contribution in the produced fluid if pore fluid is the only source of the specie

B	Br	Cl	Li	Na	K	SO4
7	4	5	8	13	9	n.a.

n.a. = not applicable.

From the results of B, Br, and Cl, we conclude that the pore fluid flow rate is approximately 4-7%. The remaining cationic species in the table probably are influenced by rock-water interactions in addition to pore fluid addition. For example, Na could be added to the produced fluid by dissolution of feldspars, and Li may undergo an ion exchange reaction in which it is liberated from the rock in exchange for Ca.

Several other dissolved species, such as Si, F, Mg, and Ca, exhibited behavior that can not be explained using a pore fluid model or a slight deviation from such a model. The easiest of these to interpret is dissolved Si, which declined in concentration only very slightly during the FWF (down to a dimensionless concentration of only about 0.95). The quartz geothermometer during steady state operation agrees with the known rock temperature in the reservoir. The nearly constant concentration during the FWF suggests that in this system the fluid has sufficient time to come to equilibrium with respect to quartz in one pass through the reservoir. This is in contrast to the Fenton Hill Phase I reservoir, showed very little active dissolution of quartz during a FWF (Grigsby and Tester, 1989). The difference in temperature (240°C versus 200°C) in the two reservoirs is apparently sufficient to cause this difference in geochemical behavior.

The behavior of fluorine was unique in that it *increased* in concentration during the test, from about 13 ppm to 15 ppm (Figure 6). The concentration of fluorine in the pore fluid was 6.1 ppm (Table 6). Assuming that this was the concentration of fluorine in the pore fluid, then this indicates the existence of another source of fluorine in addition to pore fluid. The excess of fluorine may be due to dissolution of some mineral present in the host rock (for instance mica, fluorite, or fluorapatite).

Finally, Ca and Mg exhibited a decrease in concentration despite the fact that the concentration in the injected water was *greater* than the initial concentration of these species in the production fluid. The most probable explanation for these results is the precipitation of most of the injected calcium and magnesium immediately upon entering the reservoir. Considering Ca, fluid high in concentration but low in dissolved CO_2 concentration, is being injected. When this fluid reaches the reservoir, it mixes with fluid of considerable dissolved CO_2 concentration, thereby creating a large driving force for deposition of Ca in the reservoir. Figure 7 shows the results of calculations for calcium assuming low "apparent" injection concentrations (0, 2.5 and 5 ppm, compared to the actual injection concentration of 92 ppm) for an initial output concentration of .9 ppm. Note the similarity of these curves to those of other dissolved species. This analysis suggests that the effective injection concentration of Ca after the initial deposition takes place is low, and that Ca behaves like other dissolved species thereafter.

FWF Results During Production Well Preasure Increase

Roughly 92 hours after the start of the FWF, the fluid injection pump failed temporarily, leading to a sequence of events that affected the subsequent geochemical behavior. When the injection shutdown occurred, the control system automatically increased the production well pressure to cut back on the production flow rate.

The traditional method for examining the effect of pressure and flow rate changes on hydraulic performance is to compute the impedance, defined as the pressure drop divided by production flow rate. Defined in this way, the impedance is inversely proportional to the hydraulic conductivity of the reservoir. Figure 8 shows the calculated impedance along with the production pressure during the FWF. The decrease in impedance accompanying the increase in production pressure is thought to be a result of fractures near the production well becoming more dilated at the higher pressure.

FIGURE 7. Dimensionless concentration for calcium during the FWF for different "apparent" injection concentrations

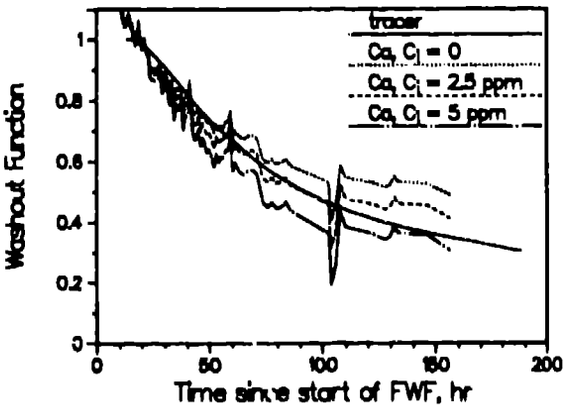

FIGURE 8. Calculated impedance and production well pressure during the FWF.

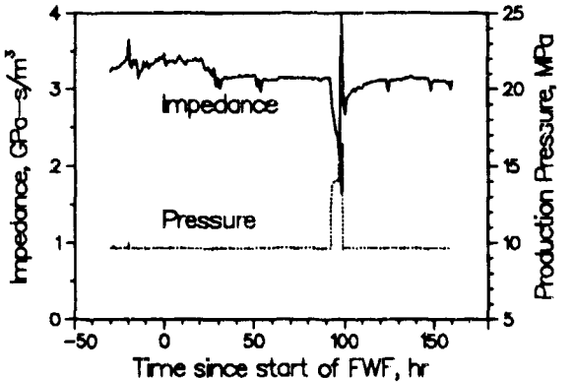

The pressure change also resulted in a short-term transient change in the chemistry of the produced fluid, as shown in Figure 9, which compares the production pressure to the fluid conductivity measurements at the surface. Increases in the pressure result in decreases in the conductivity, while subsequent decreases in pressure result in an increase to the previous conductivity level. This behavior suggests that during the FWF, the pressure rise and accompanying joint opening causes relatively fresh water to surge into the production well.

The delay time between the pressure change and subsequent conductivity change represents the transit time for a parcel of fluid to travel up the wellbore. This information allows us to pinpoint which fractures connected to the production well are opening during this pressure transient. Table 8 lists the specific pressure and conductivity changes numbered on the figure. Using a temperature log measured in the well during production, the variation of the density of the fluid with depth was calculated as a function of temperature and pressure. Then, the average travel time for a parcel of fluid from a given depth to the surface was computed. The transit time from a given depth is itself time dependent, since the flow rate was changing during the time of this analysis. Figure 10 represents the transit time for parcels of fluid entering the well at different depths. Depths chosen for the curves represent the depths of specific fluid entry positions identified from the temperature logs. The points are the transit times for the six transients identified in the fluid conductivity data.

Clearly, the uppermost fractures along the wellbore (10770 and 11050 ft) are preferentially opening, and furthermore, breakthrough of fresh water has occurred before 90 hr in these joints. However, it cannot be concluded that joints lower in the reservoir are not also undergoing this behavior, since this method can only be used to pinpoint the uppermost joints that are opening. Nonetheless, two important conclusions can be gained from this analysis. First, these uppermost joints experience breakthrough of fluid within 90 hr. There was some thought that the deepest joints, being physically closest to the fluid exit points in the injection well, might be short-circuiting flow paths that are responsible for the early residence times of the tracer breakthrough curve. Although this may still be the case, breakthrough also occurs fairly early in these upper joints. This implies that fluid sweep through the reservoir is fairly uniform. Second, increasing the production well pressure preferentially opens the upper joints, rather than simply dilating joints lower in the well, which are of most concern from the standpoint of thermal cooldown. Thus, high production well pressure does not appear to result in increased flow short-circuiting and concomitant rapid thermal decline.

FIGURE 9. Pressure and fluid conductivity during the episode of increasing production well pressure. The numbers correspond to the transients identified in Table 8.

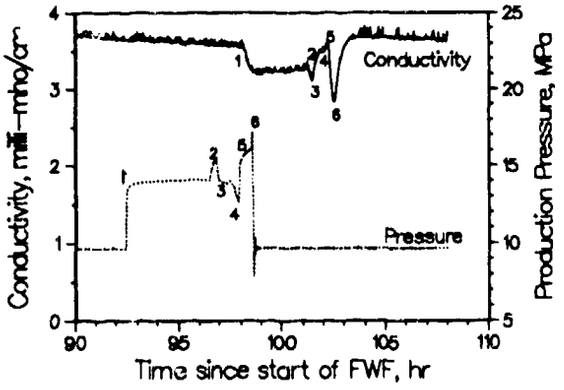

FIGURE 10. Calculated wellbore transit times from various depths to the surface. The points are the measured lag times given in Table 8.

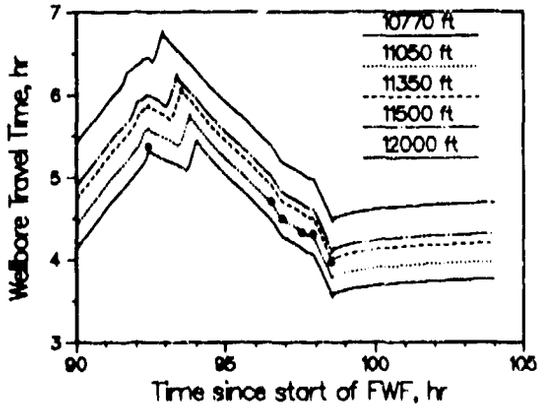

TABLE 8. Times of the Pressure and conductivity transients and lag time for displacing fluid in the wellbore (all times in hours).

Point	Pressure Time	Conductivity Time	Time Difference
1	92.43	97.8	5.37
2	96.55	101.25	4.70
3	96.90	101.40	4.50
4	97.52	101.84	4.32
5	97.89	102.20	4.31
6	98.54	102.50	3.96

Discussion and Conclusions

The three tracer experiments carried out during the LTFT have shown that the reservoir is undergoing dynamic changes during long-term heat extraction. During the 50 day period between the first and second tests, the fluid transit time in the reservoir increased markedly for the shortest residence time flow paths. This result invalidates the theory often raised in criticism of the HDR concept that heat extraction will result in the preferential opening of a short-circuiting path due to thermal contraction of the rock. The trend is in the opposite direction, toward a more uniform sweep of fluid through the rock mass. A similar phenomenon was observed in the Fenton Hill Phase I reservoir (e. g. Robinson and Tester, 1984).

The water consumed during long-term operation can, based on the measured total fracture volume, be apportioned between fluid that expands the volume of active fluid flow paths and fluid that seeps from the boundaries of the reservoir or into the rock blocks within the reservoir. A calculation based on the tracer results shows that 16% of the water loss is actually expansion of the active reservoir volume. The active fracture flow volume is also pressure-dependent: the fracture volume at a lower flow rate and pressure resulted in a lower fracture volume and more direct flow channeling between the wells.

Another use of the fracture volume measurements is to determine the nature of the pressure drop through the reservoir. The storage aperture determined from tracer measurements is at least an order of magnitude larger than the hydraulic aperture measured from pressure drop and flow rate. This result is very common in studies of flow through fractured rock (e. g. Long and Billaux, 1987, Gelhar, 1988, Robinson, 1985), and is likely due to large local pressure drops where fluid is constricted to flow through regions of small aperture. In this fracture network, there may be joints oriented unfavorably with respect to the prevailing earth stresses. These joints could dominate the pressure drop through the reservoir, while other, more open joints account for most of the fluid storage.

The FWF experiment offered a unique opportunity to explore the origins of certain dissolved species in the circulating fluid and to obtain further information about the flow patterns in the reservoir. No specie behaved as would be expected assuming no source or sink for the component. A source of the dissolved specie, postulated to be pore fluid (after Grigsby et al., 1989) is needed to explain the behavior of components such as Cl, B, and Br, which are not present in the rock minerals in sufficient quantities to be produced via dissolution or ion exchange reactions. The calculated fraction of pore fluid in the produced fluid is 4-7%. This result agrees qualitatively with the conceptual model of both direct and long-residence-time flow paths between the wells. The longer, more tortuous flow paths must be sweeping through a very large volume of rock since they are still entraining a significant amount of fluid that was in the rock mass before exploitation. These paths are probably continuously being accessed during heat extraction, and the pore fluid that originally resided in the fractures is continuously swept into the flowing fluid that reaches the production well.

Other dissolved species concentrations are influenced by rock-water interactions over the time scale of the FWF. These include Si (governed by quartz dissolution), Ca (which probably precipitated near the injection well during the FWF), and Na, which appears to have a source term in addition to pore fluid displacement. Feldspar dissolution is a likely additional source mechanism for Na.

Finally, the preferential opening of fractures near the production well was observed in both the hydraulic and geochemical data during the FWF. We were able to pinpoint the uppermost fractures that exhibited this behavior. They were the shallowest fluid entry points in the open hole, suggesting that operating at high production well pressure does not merely open the joints in closest proximity to the injection region, as might be feared. Also, the fact that these uppermost joints had already experienced breakthrough of fresh water after 90 hr shows that the flow through the rock between the wells is fairly evenly distributed.

Acknowledgments

This work was performed under the auspices of the U. S. Department of Energy, Geothermal Technology Division. N. Rodrigues would like to thank the entire staff of the EES-4 division at Los Alamos for their support and for making his stay at Los Alamos so special. Help received from D. Duchane, D. Brown, Z. Dash and R. Duteau was particularly welcome. Mr. Rodrigues' research is sponsored by the British Council (UK), University of Coimbra and INIC (Portugal). For this work he also received partial funding from the Department of Trade and Industry, UK.

References

Abelin, H., L. Birgersson, J. Gidlund, L. Moreno, I. Neretnieks, and S. Tunbrant, "Results from some tracer experiments in crystalline rocks in Sweden", in C.F. Tsang, ed. "Coupled processes associated with nuclear repositories", Academic Press, Orlando, FA, pp 363-379 (1987).

Gelhar, L. W., "Applications of Stochastic Models to Solute Transport in Fractured Rocks," SKB Technical Report 87-05, Swedish Nuclear Fuel and Waste Management Co., Stockholm, Sweden (1988)

Grigsby, C. O., J. W. Tester, P. E. Trujillo, and D. A. Counce, "Rock-Water Interactions in the Fenton Hill, New Mexico, Hot Dry Rock Geothermal Systems I. Fluid Mixing and Chemical Geothermometry", *Geothermics*, 18, 5/6, 629-656 (1989).

Grigsby, C. O., and J. W. Tester, "Rock-Water Interactions in the Fenton Hill, New Mexico, Hot Dry Rock Geothermal Systems II. Modeling Geochemical Behavior", *Geothermics*, 18, 5/6, 657-676 (1989).

Laney, R., A. W. Laughlin, M. J. Aldrich, "Geology and Geochemistry of samples from Los Alamos National Laboratory HDR well EE-2, Fenton Hill, New Mexico", Los Alamos Scientific Laboratory, Report LA-8923-MS (1981).

Long, J. C. S., and D. M. Billaux, "From Field Data to Fracture Network Modeling: An Example Incorporating Spatial Structure," *Water Resour. Res.*, 23, 7, 1201-1216 (1987).

Robinson, B. A., "Non-Reactive and Chemically Reactive Tracers: Theory and Applications", Ph.D. Thesis, Massachusetts Institute of Technology (1985).

Robinson, B. A., and P. Kruger, "Pre-Test Estimates of Temperature decline for the LANL Fenton Hill Long-Term Flow Test", Geothermal Resources Council, 1992 Annual Meeting, San Diego CA (1992).

Robinson, B. A., and J. W. Tester, "Characterization of Flow Maldistribution Using Inlet-Outlet Tracer Techniques: An Application of Internal Residence Time Distributions," *Chem. Engng. Sci.*, 41, 3 (1986).

Robinson, B. A., and J. W. Tester, "Dispersed Fluid Flow in Fractured Reservoirs: An Analysis of Tracer-Determined Residence Time Distributions," *J. Geophys. Res.*, 89, B12, 10374-10384 (1984).

Snow, D. T., "Anisotropic permeability of fractured media" *Water Resour. Res.*, 5, 1273-1289 (1969).

Witherspoon, P. A., J. S. Y. Wang, K. Iwai, and J. E. Gale, "Validity of cubic law for fluid flow in a deformable rock fracture", *Water Resour. Res.*, 16, 1016-1024 (1980).